Anharmonic Vibrational Properties of Explosives from Temperature-Dependent Raman

Shawn D. McGrane,*,† Jeffrey Barber,† and Jason Quenneville‡

Dynamic Experimentation and Applied Physics Divisions, Los Alamos National Laboratory, Los Alamos, New Mexico 87545

Received: May 4, 2005; In Final Form: August 29, 2005

Raman spectra from 50 to 3500 cm^{-1} and 4−296 K are analyzed for molecular crystal powders of the explosives pentaerythritol tetranitrate (PETN), β-octahydro-1,3,5,7-tetranitro-1,3,5,7-tetrazocine (HMX), and 1,3,5-triamino-2,4,6-trinitrobenzene (TATB) and the inert naphthalene. Temperature-dependent Raman spectroscopy is utilized for its sensitivity to anharmonic couplings between thermally populated phonons and higher frequency vibrations relevant to shock up-pumping. The data are analyzed with anharmonic perturbation theory, which is shown to have significant fundamental limitations in application to real data. Fitting to perturbation theory revealed no significant differences in averaged anharmonicities among the three explosives, all of which exhibited larger averaged anharmonicities than naphthalene by a factor of 3. Calculations estimating the multiphonon densities of states also failed to correlate clearly with shock sensitivity. However, striking differences in temperature-dependent lifetimes were obvious: PETN has long lived phonons and vibrons, HMX has long lived phonons but short lived vibrons, while TATB has short lived phonons and vibrons at low temperature. Naphthalene, widely used as a model system, has significantly different anharmonicities and density of states from any of the explosives. The data presented suggest the further hypothesis that hindered vibrational energy transfer in the molecular crystals is a significant factor in shock sensitivity.

I. Introduction

The shock initiation of detonation has been postulated to be mediated by vibrational excitation through a mechanism of multiphonon up-pumping.[1−14] In multiphonon up-pumping, a shock wave is assumed to excite only delocalized low-frequency (<200 cm^{-1}) phonons. This very hot (thousands of Kelvin) phonon bath then comes into equilibrium with the higher frequency (200−3500 cm^{-1}) intramolecular vibrations on picosecond time scales. The high-frequency vibrational excitations can then lead to chemical reactions that can (initially or after a chain of reactions) release free energy to support the shock wave until a steady reactive shock is formed and steady-state detonation proceeds. Multiphonon up-pumping is the initial step in the chain of events leading from shock to detonation.

Anharmonic interactions between vibrations are the origins of energy transfer in multiphonon up-pumping, and indeed in any vibrational process. While there are no true normal mode vibrations in anharmonic systems, the vibrations can be reasonably approximated as harmonic normal modes with anharmonic correction terms treated by perturbation theory. The anharmonicities couple different normal modes, as well as shift each normal mode energy from the harmonic value.[15−17]

If one could measure all the mode-specific anharmonicities, the time-dependent vibrational energy flow could be calculated for any initial condition. Unfortunately, there are generally $(n + r - 1)!/((n - 1)!r!)$ distinct anharmonic terms of order r (>2) for a molecule with n normal modes. For 48 normal modes there are 19 600 3rd order and 249 900 4th order constants. In solids, n will represent the number of normal modes per unit cell. Since all of these terms cannot be independently measured, approximations must be made. Time-dependent energy flow in naphthalene has been modeled by using the averaged anharmonic approximation,[18] which treats all anharmonicities with only a few constants. There have also been detailed considerations of time-dependent shock-induced up-pumping, using a single anharmonic constant determined by the average low-temperature lifetime of medium frequency doorway modes.[3] However, it was also shown that the anharmonic coupling was crucially important, and locally increased anharmonicity could account for "hot spot" regions in explosives, where the temperature (and the exponentially-dependent reaction rate) could be substantially enhanced.[3] The results of these up-pumping calculations are extremely useful in building intuition and semiquantitative properties of vibrational energy flow, and have established the formalism for understanding up-pumping processes. Unfortunately, the results can only be as accurate as the input material parameters, which are virtually unknown for explosive molecular crystals.

The temperature-dependent Raman data on explosives presented in this paper were measured to provide better input for modeling and understanding up-pumping initiation, as well as to provide experimental data for benchmarking anharmonic model calculations. Temperature-dependent Raman spectroscopy is especially sensitive to the couplings between high frequency vibrations (vibrons) and phonons that become thermally populated as the temperature rises.[15,17] Temperature-dependent vibrational spectroscopy, including time and frequency resolved Raman, infrared absorption, and neutron scattering, has been frequently utilized to measure properties of vibrational energy flow and lattice dynamics in molecular crystals. These studies have included temperature-dependent Raman spectroscopy of the explosives 1,3,5-triamino-2,4,6-trinitrobenzene (TATB),[13,19−22] 1,3,5-trinitro-*s*-triazine (RDX), β-octahydro-1,3,5,7-tetranitro-1,3,5,7-tetrazocine (HMX), and tetryl crystals,[10,11] as well as

† Dynamic Experimentation Division.
‡ Applied Physics Division.

10.1021/jp0523219 CCC: $30.25
Published on Web 10/18/2005

various experimental techniques studying vibrational dynamics in naphthalene[15,17,23−34] and other molecular crystals.[17,35−43]

In this paper, we analyze the temperature-dependent Raman scattering of pentaerythritol tetranitrate (PETN), β-octahydro-1,3,5,7-tetranitro-1,3,5,7-tetrazocine (HMX), and 1,3,5-triamino-2,4,6-trinitrobenzene (TATB) in search of features that strongly differ between these molecular crystals that have very disparate shock sensitivities. Temperature-dependent Raman data on the inert material naphthalene are also presented for comparison, specifically to show that this model system is measurably vibrationally dissimilar to the explosive molecules. The analysis of the temperature-dependent line widths with perturbation theory is reported, but the severe limitations of applying anharmonic perturbation theoretical expressions to real data are also examined. There are substantial differences in the temperature-dependent line widths that can be interpreted without the assumptions or limitations of the perturbation theory analysis. In interpreting the origin of the differences observed in the line width data, we consider both the anharmonicities and the multiphonon densities of states for each molecular crystal.

II. Theory

A. Anharmonic Perturbation Theory and Vibrational Up-Pumping. All interpretation of the data considered here is based on the results of anharmonic perturbation theory.[15,17,44,45] In the equations below, all fundamental and numerical constants have been absorbed into the anharmonicity constants, and all line widths given are full width at half-maximum for Lorentzian line shapes. The word phonon will often be used for localized vibrations or vibrons as well as for truly delocalized phonons, since they are treated equivalently.

The lowest order perturbation leads to the frequency shift $\Delta_\omega(T)$ from a harmonic frequency ω, due to elastic scattering with virtual phonons. The frequency shift is given by eq 1, where the scattering phonon is of frequency ω_i and occupation number $n_i = (\exp(\hbar\omega_i/kT) - 1)^{-1}$, where k is Boltzmann's constant, and $A_{i,\omega}$ is a mode specific 4th order coupling coefficient, which can be positive or negative.

$$\Delta_\omega(T) = \sum_i A_{i,\omega}(2n_i + 1) \tag{1}$$

Unfortunately, eq 1 is for constant volume,[15,24,31,46] while experiments are performed at constant pressure. Since the temperature-dependent volume corrections cannot be made accurately for the materials considered here, we do not report any quantitative analysis of the temperature-dependent frequency shifts observed.

The next term in the perturbation expansion accounts for the increase in line width $\Gamma_\omega(T)$ with temperature, as given by eq 2, where $B^{(3)}_{j,k,\omega}$ is a 3rd order anharmonic coupling constant and the δ function enforces energy conservation. Momentum conservation is implicit for notational simplicity, but must be considered for phonons with considerable dispersion.

$$\Gamma^{(3)}_\omega(T) = \sum_{j,k} |B^{(3)}_{j,k,\omega}|^2[(n_j + n_k + 1)\delta(\omega - \omega_j - \omega_k) + (n_j - n_k)(\delta(\omega - \omega_j + \omega_k) - \delta(\omega + \omega_j - \omega_k))] \tag{2}$$

The $(n_j + n_k + 1)$ term of eq 2 corresponds to stimulated and spontaneous phonon emission, together called down-conversion. The second term $(n_j - n_k)$ corresponds to a given phonon scattering from a lower frequency phonon to form a single phonon of higher frequency, called up-conversion. The temperature dependence is contained in the occupation number of the scattering phonons. The sum of all spontaneous down conversion terms accounts for the $T = 0$ line width.

Higher order terms have been shown to include pure dephasing and higher order relaxation effects (>3 phonon scattering).[15,24,37,47] A pure dephasing term is occasionally employed[10,11,24,32] in the form given by eq 3 when the temperature dependence does not become linear at high temperatures, where $B^{(4)}$ is a fourth order anharmonic coupling and the wavevector dependence is again implicit.

$$\Gamma^{(4)\text{dephasing}}_\omega(T) = \sum_k |B^{(4)}_{k,k,\omega,\omega}|^2 n_k(n_k + 1) \tag{3}$$

There are many higher order terms, which are of functional forms too complex to reasonably fit to experimental data and by necessity assumed to be negligible.

Most experimental data are remarkably well fit by the simplified fitting form of eq 4, which assumes a single up-conversion $B^{(4)}_u$and down-conversion $B^{(4)}_d$ pathway.

$$\Gamma^{(3)\text{fit}}_\omega(T) \equiv \Gamma(0) + |B^{(3)}_d|^2(n_j + n_k + 1)\delta(\omega - \omega_j - \omega_k) + |B^{(3)}_u|^2(n_l - n_m)\delta(\omega + \omega_l - \omega_m) \tag{4}$$

A simplified form that includes a single dephasing pathway, given by eq 5, is also considered in the Results Section C, where the limitations of fitting to eqs 4 and 5 are examined in detail.

$$\Gamma^{(4)\text{fit}}_\omega(T) \equiv \Gamma^{(3)\text{fit}}_\omega + |B^{(4)}_p|^2 n_k(n_k + 1) \tag{5}$$

The mode-specific temperature-dependent up-pumping rate relevant to shock initiation is given by just the part of eq 2 isolated in eq 6, where a vibration of frequency ω_k is created by the annihilation of two lower frequency phonons.

$$k^{(3)\text{up}}_{i+j\rightarrow k}(T) = |B^{(3)}_{i,j,k}|^2\delta(\omega_i + \omega_j - \omega_k)(n_j - n_k) \tag{6}$$

Up-pumping often considers the entire flow of population from all the thermally excited phonons into a given vibration. Summing over all i and j in eq 6 and extending consideration to a continuous distribution of phonons gives eq 7. In eq 7 all normalization constants are absorbed into the anharmonicity constant, for simplicity.

$$k^{(3)\text{up}}_{\rightarrow k}(T) = \int_0^\omega d\omega_i |B^{(3)}_{i,j,k}|^2 \rho(\omega_i)\rho(\omega - \omega_i)(n_i - n_k) \tag{7}$$

Equation 7 is presented simply to show that the squared anharmonicity constants that determine low-temperature vibrational relaxation are the same as those involved in up-pumping, and to illustrate the importance of the two-phonon density of states. The two-phonon density of states, defined in eq 8, serves as the final states excited by down-conversion or the initial states for up-conversion.

$$\rho^{(2)}(\omega) = \int_0^\omega d\omega_i \rho(\omega_i)\rho(\omega - \omega_i) \tag{8}$$

The total energy flow into a vibration at short times (neglecting back action) determined from eq 7 is of the same functional form as that derived by using the Fermi Golden Rule[5] under similar circumstances (keeping the up-pumping term only, negligible occupation of high-frequency vibrations compared to phonons).

B. Multiphonon Density of States Calculations. Equation 8 is similar to the more general case of eq 2.5 of DellaValle,[48]

rewritten in our notation for consistency in eq 9.

$$\rho^{(n)}(\omega) = \int_0^{\omega} d\omega_i \rho^{(n-1)}(\omega_i)\rho^{(1)}(\omega - \omega_i) \qquad (9)$$

Equation 9 allows one to calculate successfully higher order density of states starting with $\rho^{(1)}(\omega)$. This method has the advantage of scaling only with the resolution of $\rho^{(1)}(\omega)$, and not with n. A simple program was written to perform these calculations.

To this end, it was necessary to determine the one-phonon density of states for each of the materials of interest. For a molecule of N atoms in a crystal with a unit cell containing Z molecules, there should be $3NZ$ modes: 3 acoustic phonons, $Z(3N - 6)$ vibrons and $6Z - 3$ optical phonons.[36] Much of the information needed to accurately determine the one-phonon density of states is not accessible, requiring certain assumptions to be made to enable a consistent comparison between molecules. For acoustic phonons, we assumed a Debye distribution and Debye frequency of 100 cm^{-1}. For optical phonons, a uniform distribution from 0 to 200 cm^{-1} with an integrated area equaling $6Z - 3$ phonons was assumed.

Vibrational frequencies calculated at the B3LYP[49,50]/6-31G* [51−55] level were used, combined with assigned frequencies where practical from published calculations for HMX[56] and PETN.[57] Due to the lack of recently published calculated frequencies for TATB, a comprehensive study was initiated with use of ab initio and density functional theory methods, the results of which will be published separately. For this work, TATB was geometry optimized in a vacuum, using the Gaussian03[58] electronic structure program, with the B3LYP density functional and the 6-31G* basis set. The optimization started from a nonplanar configuration and no symmetry restrictions were applied to either the wave function or the geometry. The optimized geometric parameters were similar to those obtained by Manaa and Fried,[59] using the same functional but a larger basis set. Vibrational frequencies were then calculated within the harmonic approximation, using the same method and basis set (B3LYP/6-31G*), and the calculated frequencies were left unscaled.

The phonons below 200 cm^{-1} were given a width of 15 cm^{-1}, while those above 200 cm^{-1} were given a width of 4 cm^{-1} to approximate the effects of dispersion and the room temperature line widths in the solid. Diffraction data[60−64] were used to calculate the unit cell volumes for all materials for density of states normalization. The one-phonon density of states was scaled to give units of states/cm^3. This scaled $\rho^{(1)}(\omega)$ was then used to calculate $\rho^{(2)}(\omega)$, $\rho^{(3)}(\omega)$, and $\rho^{(4)}(\omega)$ by numerical solution of eq 9.

III. Experimental Section

Details of the temperature-controlled Raman apparatus have been reported previously.[13] The 514.53 nm line of an argon ion laser was isolated and <100 mW focused on a capillary tube of powdered crystal mounted in a continuous flow liquid helium cryostat with a helium exchange gas in contact with the sample. Scattered light was collected at ~170°, passed through a holographic notch filter, and focused on a 40 μm (25 μm for naphthalene) entrance slit of a 1 m Spex single grating (1800 g/mm) spectrometer. A liquid nitrogen cooled CCD detected the spectrally resolved light in 1152 vertical bins with integration times typically of 50 s per spectral window (spectral windows recorded every 15 nm). Samples were standard grade crystalline powders of HMX and PETN used as drop test standards, and scintillation grade (99+%) naphthalene. HMX and PETN spectra have been baseline subtracted, which is only significant below ~100 cm^{-1}. TATB data were reported in ref 13.

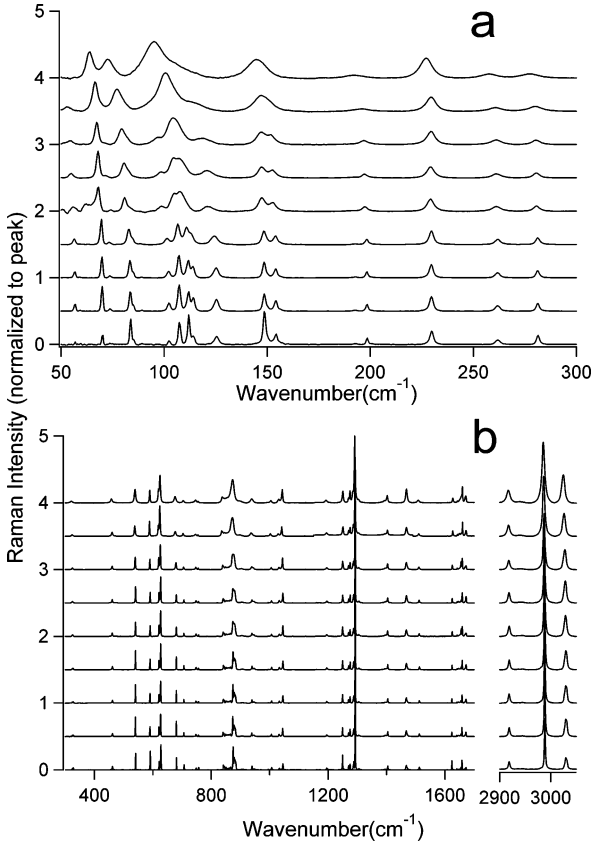

Figure 1. Raman spectrum of PETN at 296, 225, 151, 121, 101, 58, 30, 15 and 7 K (from top to bottom): (a) magnification of the phonon region and (b) higher frequency fundamental region.

Calibration at each spectral window and the instrumental response function were determined with emission lines from a Ne[65] spectral lamp. Absolute frequencies are only accurate to ±1 pixel, which ranges from 0.43 cm^{-1} near zero frequency to 0.29 cm^{-1} near 3200 cm^{-1}. Peaks were fit to a Lorentzian functional form numerically convoluted with the instrumental response for determination of line widths. TATB line widths were redetermined by fitting original data including the convolution with instrumental response (convolution was not included in ref 13) as determined from the original Ne calibration lines taken at the same time as the data. Line widths determined in this manner seem to be adequate for lines >0.25 cm^{-1}. Narrower lines depend too strongly on fitting the wings or tail of the peaks and are not reliably determined.

IV. Results

A. Raman Spectra. The Raman spectra of PETN at nine fixed temperatures are shown in Figure 1. Figure 1a shows an expansion of the region below 300 cm^{-1}, while Figure 1b shows higher frequency Raman active vibrations. Figures 2−4 show the temperature-dependent Raman data in the same format for HMX, TATB, and naphthalene, respectively. The TATB data are the same as those reported in ref 13, but are repeated here for ease of comparison with the other data in the considerations in the Discussion section.

No clearly identifiable peaks were found between 1700 cm^{-1} and the high-frequency stretches above 2700 cm^{-1} in any of the compounds studied except for naphthalene, which exhibited numerous low intensity peaks, typically $<2 \times 10^{-3}$ of the strongest peak signal.

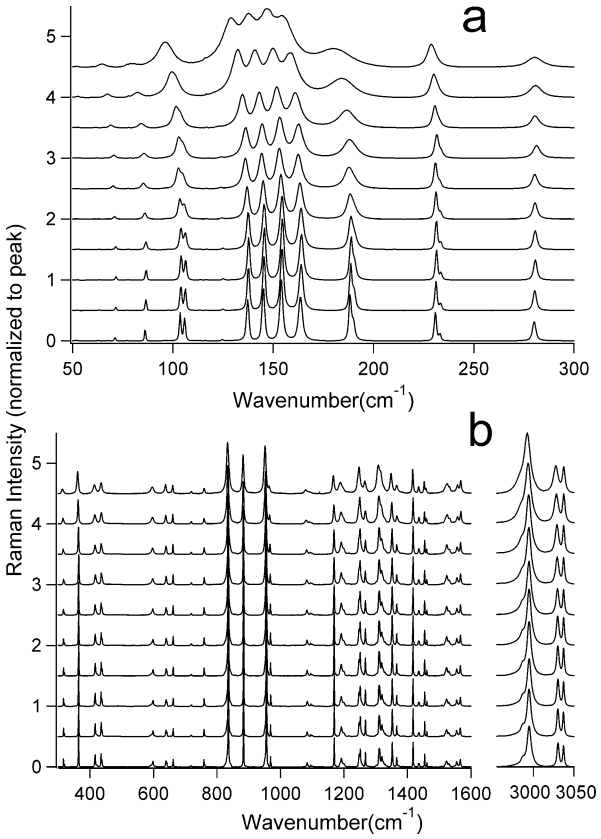

Figure 2. Raman spectrum of HMX at 296, 225, 150, 127, 100, 74, 50, 27, 13, and 7 K (from top to bottom): (a) magnification of the phonon region and (b) higher frequency fundamental region.

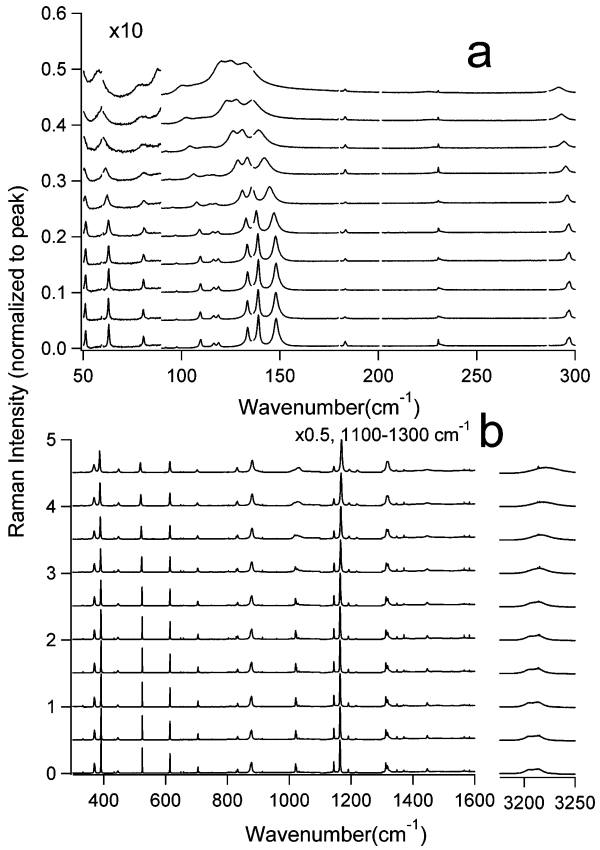

Figure 3. Raman spectrum of TATB at 295, 250, 200, 150, 101, 62.0, 32.8, 15.7, 8.05, and 3.90 K (from top to bottom) from ref 13: (a) magnification of the phonon region and (b) higher frequency fundamental region.

B. Fitting to Anharmonic Perturbation Theory. All the line width data that could be reliably extracted over at least a temperature range up to 100 K were tabulated and fit to eq 4. Only peaks reliably fit with Lorentzian line shapes were tracked. This included peaks that overlapped, as long as the sum of Lorentzians adequately described the data. Even keeping only the best fit peaks, we report in Table 1 only the averaged anharmonic constants for 3-phonon down-conversion derived from fitting to eq 4. Up-conversion was simultaneously fit, but we felt that the parameters were not as reliably determined since at low temperatures, the occupation numbers are small.

C. Model Calculations Showing Limitations of Anharmonic Perturbation Theory. Calculations were performed to test the limitations of fitting perfect data generated numerically from eq 2 to the simplified fitting form of eq 5. A few simple parameter sets were chosen, labeled models i−iv in Table 2 and corresponding to Figure 5b curves i−iv.

The temperature dependence was assumed to be strictly due to the occupation number (no temperature-dependent anharmonic constants). The temperature dependence of the Bose−Einstein occupation number for 100, 200, and 300 cm^{-1} modes is shown in Figure 5a for reference. Models i and ii are identical, and simply fit with different assumptions. Model i/ii has only two virtual scattering phonons with equal up- and down-conversion anharmonic constants and no dephasing. Fit 1 assumes a single scattering frequency and allows fitting different anharmonicity constants for up- and down-conversion. Fit 2 assumes no up-conversion, but is found to also fit essentially perfectly (maximum deviation <0.02 cm^{-1}). Model iii illustrates that even four scattering phonons can be fit essentially perfectly with the single frequency form of eq 4 or eq 5. Models i−iii would also have fit identically to eq 4, since the dephasing constant was determined to be zero in the fitting. Model iv illustrates that more disparate scattering frequencies can also lead to a curvature with temperature that can be misidentified as dephasing, when fit to eq 5. All the numerically generated input data and the fits over the range 0−300 K are shown in Figure 5b.

D. Three Temperature Line Width Spectra. Figure 6 shows the dephasing lifetime spectrum for each material at 4−7, 100−101, and 291−296 K. This was calculated from the line width, Γ, by the equation $T_2 = 1/(\pi c\Gamma)$ for the lines which could be well fit to Lorentzian functions at all temperatures. Reasons for displaying these three temperatures and the significance of the differences between molecules apparent in Figure 6 are discussed in Discussion Section D.

E. Multiphonon Densities of States. The one-phonon and multiphonon ($N > 1$) densities of states (DOS) were calculated as described in Theory Section B. The resulting $N = 1$ DOS for the materials of interest are shown in Figure 7, with curves offset for clarity. The two-phonon DOS are presented in Figure 8. Finally, Figure 9 shows the DOS for $N = 1-4$ for HMX.

V. Discussion

A. Raman Spectra. The low-temperature spectra clearly resolve many peaks that are unresolved at room temperature. However, all of the spectra exhibit regions of overlapping peaks that could not be resolved even at the lowest temperatures. These unresolved peaks can be caused by either large spectral density or inhomogeneous broadening. The main qualitative difference between molecular crystal spectra apparent from examination of Figures 1−4 is that naphthalene has significantly sharper peaks than the other molecules.

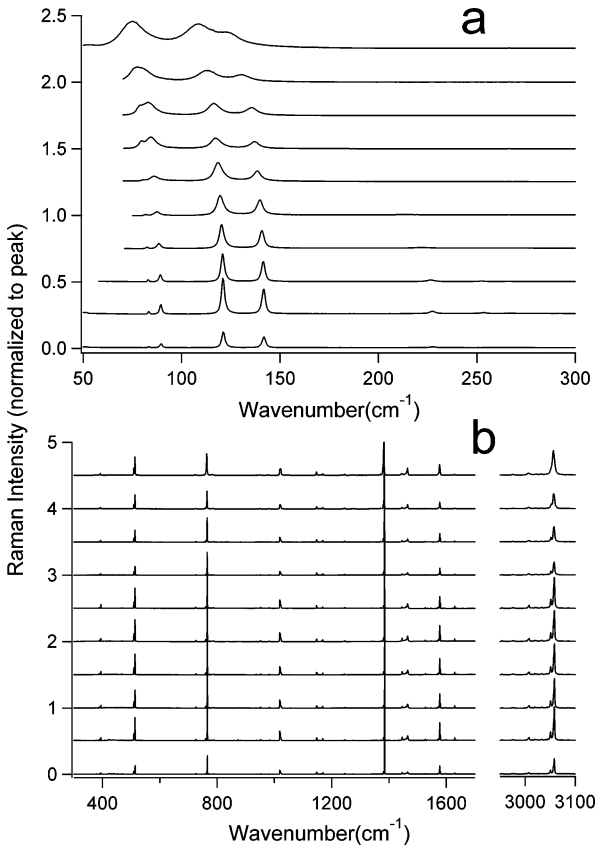

Figure 4. Raman spectrum of naphthalene at 291, 221, 148, 121, 100, 78, 50, 25, 13, and 6 K (from top to bottom): (a) magnification of the phonon region and (b) higher frequency fundamental region.

TABLE 1: Average and Maximum Down Conversion Anharmonic Coupling Constants from the Fit to Eq 4[a]

$B_d^{(3)}$ (cm^{-1})	PETN	HMX	TATB	naphthalene
average	0.99	0.82	0.96	0.36
maximum	2.6	2.4	6.7	1.8
no. of peaks fit	13	24	19	23

[a] All line widths that were adequately resolved from nearby peaks over a temperature range up to at least 100 K.

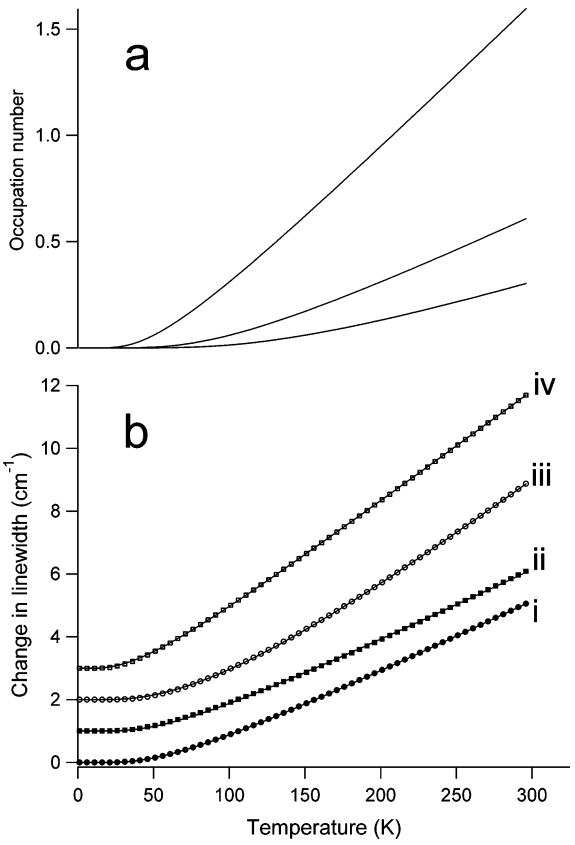

Figure 5. (a) Occupation number versus temperature for vibrational frequencies of 100, 200, and 300 cm^{-1} (from top to bottom), illustrating the narrow temperature range over which a vibration's occupation number passes from no temperature dependence, to nonlinear increase, to linear increase. (b) Calculated temperature-dependent line widths calculated from eq 2 (solid lines) and fits to eq 5 (open and closed circles and squares). Input and fit parameters are given in Table 2 as models i−iv and fits i−iv, corresponding to annotations i−iv on plot. Curves are offset from zero for clarity. The largest discrepancy observed in any of these fits is 0.04 cm^{-1}, significantly less than typical experimental line width noise, despite fitting multiple scattering frequencies as if a single scattering frequency was present, and having extra (pure dephasing) or fewer (no upconversion) physical processes in the fit than present in generating the data.

The low-temperature spectra should be useful as a benchmark for calculations of the fundamental vibrational frequencies. The temperature dependence of the vibrations may also serve to critically test calculations using anharmonic potentials. While anharmonic molecular calculations in condensed phases are extremely challenging, they may offer the only hope of achieving reasonably accurate values for the tremendous number of anharmonic constants for the molecular crystals considered here.

B. Fitting to Anharmonic Perturbation Theory. The reasons for limiting the presentation of fit parameters to those given in Table 1 are 2-fold: First, the fitting process offers only a weighted average of anharmonic constants and frequencies (as discussed in the next section). Second, the conclusions from looking at the fit parameters of all 79 peaks are summarized well by the data shown in Table 1. Namely, the fit anharmonic constants are very similar for the three energetic materials, but those anharmonicities are approximately a factor of 3 larger than that for naphthalene. The approximately 1 cm^{-1} third-order anharmonic constants determined here are very similar to the three phonon anharmonic couplings observed for the energetic materials HMX, RDX, and tetryl.[10,11] The only outlier in our analysis is the NH stretch of TATB at ∼3200 cm^{-1}, which has a very strong 3-phonon anharmonic coupling, fit as ∼6.7 cm^{-1}. This is likely to originate in the extensive intra- and intermolecular hydrogen bonding between the amine and nitro groups in TATB. While we could not determine anharmonicities for every vibration, we have followed a reasonable number that encompass the entire energy range of the vibrational fundamentals.

C. Limitations of Fitting Data to Anharmonic Perturbation Theory. Table 2 and Figure 5 illustrate why eqs 4 and 5 describe the temperature-dependent Raman data of many molecular crystals so well: the fitting is not very sensitive. While the real materials will have thousands of terms in the summation of eq 2, the temperature dependence over a limited range will select out several terms, and the fit will give results that are essentially a weighted (by the multiplicative anharmonic constant and nonlinearly by the occupation numbers) average over these several terms. Figure 5a shows why only a limited number of terms contribute. The temperature dependence of the occupation number changes from negligible to nonlinear to linear over a very localized range of temperatures. Equations 4 and 5 are only sensitive to this region of curvature. If the curvature is localized due to a number of similar contributing frequencies, a single fit frequency can be found, as in models

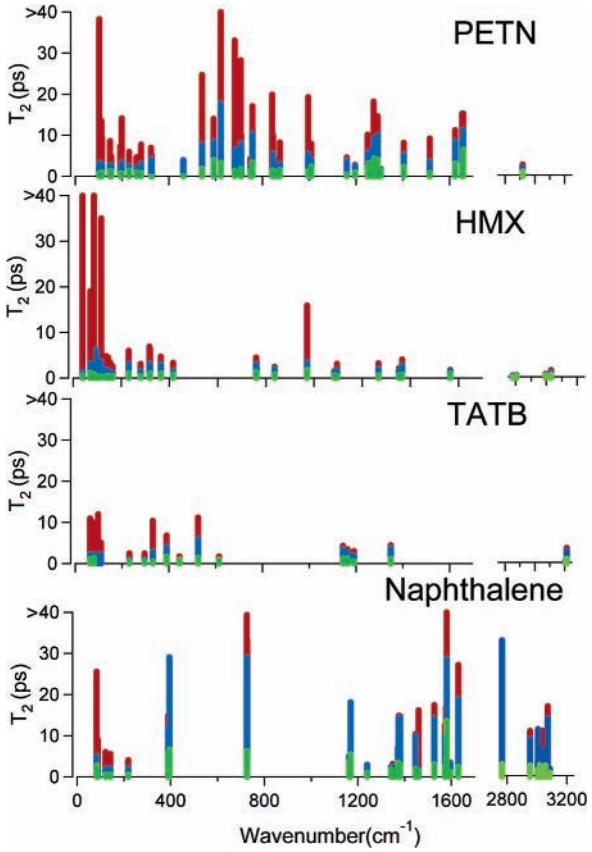

Figure 6. Dephasing time spectra from inverse Raman line widths for three temperatures: red, 4−7 K; blue, 100 K; and green, 295 K. Dephasing times over 40 ps were not resolved with our spectral resolution.

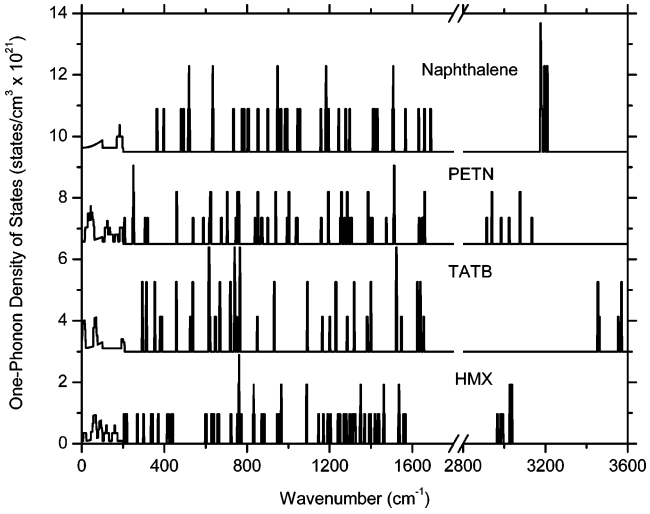

Figure 7. Calculated one-phonon density of states for naphthalene, PETN, TATB, and HMX. Curves are offset for clarity.

i−iii of Table 1. If there is a disparate frequency scatterer, multiple regions of curvature will be present and the temperature dependence will not become linear quickly. This can easily be mistaken as a sign that higher order dephasing is present (as in eq 5), which also induces curvature over a larger temperature range than single frequency up- or down-conversion. This is quantified for a simple example in model iv, which mistakes multiple frequencies for dephasing, even with numerically generated data that have no noise.

With these severe ambiguities, is there any value in fitting data to anharmonic perturbation theoretical expressions? There

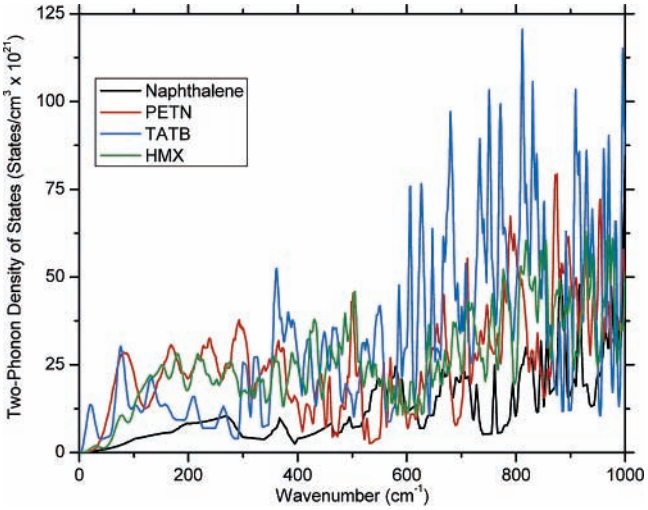

Figure 8. Calculated two-phonon density of states for naphthalene, PETN, TATB, and HMX in the region 0−1000 cm^{-1}.

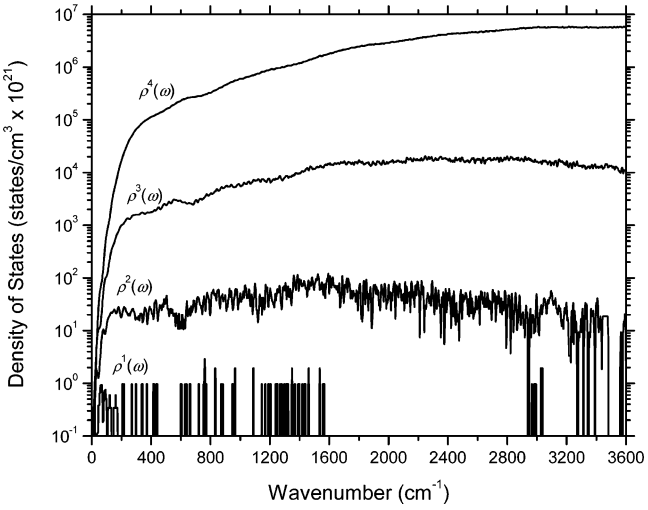

Figure 9. Calculated one-, two-, three-, and four-phonon density of states for HMX.

can be some value in the parameters determined from the fits. If a very small number of pathways can be identified, as for phonon decay in naphthalene, the contributions from each pathway can be identified, although dispersion complicates the analysis. Even for more complex cases such as the higher frequency vibrations studied here, the fit to eq 4 will determine values indicative of the sum of anharmonic constants weighted by their occupation number terms and energy conservation. While this is not the mode specific anharmonicity that is desirable, it does provide upper bounds on individual anharmonic constants that contribute to the sum. Additionally, the curvature indicates the range of dominant frequencies contributing to the sum. The anharmonic perturbation theory provides the relevant conceptual basis for understanding vibrational energy transfer in molecular crystals; it is simply the insensitivity of fitting actual data to the equations that is the limitation.

D. Three Temperature Line Width Spectra. Anharmonic differences between the molecular crystals studied here are apparent from the temperature-dependent line widths, without the limitations of anharmonic perturbation theory. The dephasing time, or inverse line width, data are shown in Figure 6 for three temperatures. The homogeneously broadened Raman line widths $\Gamma = 1/(\pi c T_2)$ are determined by dephasing time T_2, which can contain contributions from T_1 (vibrational energy relaxation) and T_2^* (pure dephasing) where $1/T_2 = 1/(2T_1) + 1/T_2^*$.

TABLE 2: Three Sets of Input Parameters Used To Calculate Temperature-Dependent Line Widths from Eq 2, and the Resulting Four Sets of Fit Parameters to Eq 5[a,b]

ω_i	ω	$B^{(3)}_d$	$B^{(3)}_u$	$B^{(4)}_d$	max deviation
	model i = model ii				
100	400	1	1	0	
150	400	1	1	0	
fit i					
114.7	400	*2.1*	*1.62*	*0*	0.004
fit ii					
100.6	400	*2.905*	*0*	*0*	0.02
	model iii				
50	400	1	1	0	
75	400	1	1	0	
100	400	1	1	0	
125	400	1	1	0	
fit iii					
71.3	400	*2.26*	*1.28*	*0*	0.04
	model iv				
100	400	1	1	0	
150	400	1	1	0	
300	400	3	3	0	
fit iv					
129.5	400	*5.05*	*0*	*0.114*	0.02

[a] Fit ii uses the same input data as fit i but assumes no up-conversion. [b] All units are in cm^{-1}, parameter values fit to eq 5 are in italics, model labeling corresponds to Figure 5b, where fits are shown.

However, in low-temperature molecular crystals, the vibrational dephasing observed in Raman line widths can be attributed solely to T_1 processes. This is expected since pure dephasing is a higher order correction in perturbation theory. Dephasing has been suggested to become significant at $\leq$100 K from temperature-dependent Raman studies.[10,11,32] However, the curvature of the temperature dependence due to dephasing may be overestimated, since it cannot be easily distinguished from third order anharmonic coupling to multiple frequencies, as discussed in the previous section. Most of our data were fit well to >100 K with a single frequency in eq 3, indicative of the lack of dephasing, and much of the data were well fit with a single frequency to room temperature. While dephasing cannot be conclusively distinguished from multiple frequency scattering, the lack of dephasing can be identified by temperature-dependent Raman spectroscopy.

The three temperatures shown in Figure 6 were chosen for the following reasons: The low-temperature data are essentially the $T \rightarrow 0$ K limit of eq 2, the 100 K data are reasonably expected to be affected only by T_1, and room temperature is the typical initial state for shock initiation, although the line width may be affected by pure dephasing. Note that the dominance of T_1 in molecular crystals contrasts with the dominance of T_2* in liquids where diffusion and rotation lead to a fluctuating intermolecular potential that induces dephasing in addition to purely anharmonic effects.

Figure 6 shows that the low-temperature lifetimes of phonons are longest in HMX, PETN, and naphthalene (which also has two Raman active phonons[24,29,33,36] with lifetimes well over 40 ps at 57 and 68 cm^{-1} which were not tracked here), while TATB has only short-lived (<15 ps) phonons at 4 K. The low-temperature vibron lifetime spectrum shows many long-lived (>15 ps) vibrons in PETN and naphthalene, but very few in HMX and none in TATB. Recall that the low-temperature lifetimes are affected by the summation of all decay modes in eq 2.

The change from the low-temperature to 100 K lifetime in Figure 6 is affected by the summation of couplings to low-frequency phonons below ~200 cm^{-1} (see Figure 5a) in eq 2. These frequencies are the most delocalized and expected to be most important in shock-induced up-pumping. All the phonons below ~200 cm^{-1} have their lifetimes significantly decreased, as expected due to the increased stimulated phonon emission of lower frequency phonons. For higher frequency vibrons, PETN exhibits the largest absolute drop in lifetimes. Many of naphthalene's vibrons see very little change in lifetime, suggesting very weak vibron−phonon coupling. HMX and TATB had such short low-temperature vibron lifetimes that the spontaneous down-conversion between vibrons seems to dominate stimulated down-conversion.

At room temperature, PETN, HMX, and TATB line widths exhibit changes similar to those observed upon changing from low temperature to 100 K. Naphthalene finally displays vibrons substantially losing lifetime between 100 K and room temperature, indicating that thermal activation of higher frequency (>200 cm^{-1}) modes is required to significantly limit lifetime.

In summary, our interpretation of Figure 6 in terms of relative phonon (<200 cm^{-1}) and vibron (>200 cm^{-1}) coupling strengths is the folowing: (1) PETN has weak vibron−vibron couplings and strong phonon−vibron couplings, (2) HMX has strong vibron−vibron couplings and moderate phonon−vibron couplings, (3) TATB has strong vibron−vibron couplings, moderate phonon−vibron couplings, and the strongest phonon−phonon couplings, and (4) naphthalene has weak vibron−vibron couplings and weak phonon−phonon couplings. The vibron−vibron couplings are indicated by the low-temperature vibron lifetimes. The vibron−phonon couplings are indicated by the change in lifetimes from low temperature to 100 K. The strong phonon−phonon couplings in TATB are indicated by the relatively short low-temperature lifetime of its phonons. Note that Figure 6 only shows the Raman active modes well fit to a homogeneous line width. All modes could not be followed, but we tried to track enough vibrations to be representative across the entire fundamental vibrational spectrum.

E. Multiphonon Densities of States. The 3 temperature lifetime spectra show significant differences between the 4 molecular crystals studied. Do these differences originate in significantly different anharmonic constants, different multiphonon densities of states (DOS), or both? Fitting to anharmonic perturbation theory suggested that PETN, HMX, and TATB all have similar anharmonic constants, while naphthalene's are much smaller. Figure 8 suggests that PETN and HMX have very similar DOS, while TATB has a slightly lower DOS at frequencies ~100−300 cm^{-1} and more pronounced structure at higher frequencies. Naphthalene has a substantially smaller DOS. The interpretation of naphthalene is then the simplest: both the DOS (originating largely in the relatively low crystal density) and the anharmonicities are much smaller those of the explosive molecules, and the vibrational lifetimes are correspondingly longer. The fact that HMX and PETN have similar DOS, but PETN has much longer vibron lifetimes, suggests that the vibron anharmonicities are substantially greater in HMX, even though this was not apparent in the perturbation theory fits. Also, the TATB DOS should allow longer lifetimes than PETN and HMX since there is a smaller average DOS in the region below 200 cm^{-1}, but this is apparently overwhelmed by larger anharmonicities. Again, the larger anharmonicities in TATB were not apparent in the perturbation theory fits.

While a number of approximations needed to be made to estimate the DOS, the fine details are not crucial for the gross considerations here. Moderate frequency errors do not affect the DOS much, and less so for the multiphonon DOS where details become washed out. The dominant factor affecting the low-frequency DOS is the number of intramolecular vibrations

that are amalgamated into the phonons at <200 cm^{-1}. The number of amalgamated vibrons is 32 for PETN, 22 for HMX, 14 for TATB, and only 4 for naphthalene, all doubled from the single molecule calculation since all of these crystals have 2 molecules per unit cell. Consequently, the two-phonon DOS in the region below 400 cm^{-1} is very different for naphthalene than for the other molecules. This is clearly seen in Figure 8, with naphthalene having about half the states available to HMX, PETN, and TATB.

Figure 9 shows the $N = 1-4$ DOS for HMX. Above $N = 2$, most of the structure has been washed out due to the increasing number of combinations possible. Figure 9 is typical of the $N = 1-4$ DOS for TATB, PETN, and naphthalene, with the differences in $N = 1$ DOS for the different materials propagating into the higher orders. The multiphonon DOS for 1,3,5-trinitro-1,3,5-triazocyclohexane or RDX ($Z = 8$) was also calculated to observe the effects of the difference in Z. RDX DOS was very similar to HMX, as expected since the acoustic phonon density plays a very small role.

F. Applicability of Data toward Multiphonon Up-Pumping. The molecular crystals studied here have very different reactive properties under shock loading. For a 4 GPa input shock the run distance to detonation is approximately 16 mm for TATB, 7−12 mm for different densities of PBX 9501 (95% HMX), and ∼1.5 mm in pressed PETN.[66] The drop height at which an event occurs 50% of the time under defined (Type 12) impact test conditions for PETN, HMX, and TATB has been reported as 12, 26, and >320 cm, respectively.[66] These are only two of a myriad of methods describing the relative sensitivities, which all consistently rank PETN as far more sensitive than HMX, which in turn is far more sensitive than TATB to external stimuli. Naphthalene is not an explosive, and its reactivity under shock conditions is not known. Even if naphthalene decomposes quickly upon shock loading, it simply does not release the chemical energy required at a sufficient rate to form a self-supporting detonation wave.

The vibrational lifetimes are significantly different for these four molecular crystals. This seems to originate in the anharmonicities and not in the vibrational DOS, with the exception of naphthalene, which has lower anharmonicities and DOS. The anharmonicities in TATB are apparently significantly larger than HMX, which are larger than in PETN, which are larger than in naphthalene. The correlation of vibrational lifetime with shock sensitivity in the explosives suggests that hindered vibrational energy flow can lead to energy localization that enhances chemical reactivity leading to detonation.

The correlation between vibrational lifetime and shock sensitivity does not identify cause and effect. Detonation is a complicated phenomenon that involves rate of multiphonon up-pumping, rates of chemical reaction, energy release, heating and expansion, and coupling of the energy back into a traveling shock front. The data presented here are only directly related to the initial up-pumping phenomena.

Much of what we see in the vibrational lifetimes matches expectations. TATB has extensive hydrogen bonding that presumably facilitates energy flow. PETN has low-frequency torsions that can couple energy from phonons into vibrons (though the long lifetimes in PETN were not obviously expected). Naphthalene has a much simpler molecular structure with smaller bond dipoles (only C and H atoms) and would be expected to have weaker vibrational coupling.

VI. Conclusions

Temperature-dependent Raman and calculated multiphonon densities of states were analyzed to seek correlations of anharmonic vibrational properties with sensitivity to shock initiation. Fitting data with anharmonic perturbation theory was performed, but determined to be inadequate to characterize anharmonic couplings. Numerical analysis of the perturbation theory equations verified that the mathematical expressions were simply not sensitive enough to temperature-dependent line widths to accurately determine the fit parameters. Even without quantification of anharmonic parameters due to the limited sensitivity of perturbation theory, large discrepancies in temperature-dependent lifetimes were observed. The multiphonon densities of states were estimated, and found to be similar for the different explosives studied and significantly lower for naphthalene, implying that a major cause of lifetime variations in the explosives originates in the anharmonic coupling constants. From the spectra of lifetimes at approximately 6, 100, and 295 K, relative phonon (<200 cm^{-1}) and vibron (>200 cm^{-1}) coupling strengths were determined: (1) PETN has weak vibron−vibron couplings and strong phonon−vibron couplings, (2) HMX has strong vibron−vibron couplings and moderate phonon−vibron couplings, (3) TATB has strong vibron−vibron couplings, moderate phonon−vibron couplings, and the strongest phonon−phonon couplings, and (4) naphthalene has weak vibron−vibron couplings and weak phonon−phonon couplings. The vibron−vibron couplings are indicated by the low-temperature vibron lifetimes. The vibron−phonon couplings are indicated by the change in lifetimes from low temperature to 100 K. The strong phonon−phonon couplings in TATB are indicated by the relatively short low-temperature lifetime of its phonons. The correlation of vibrational lifetimes with shock sensitivity in the explosives suggests the hypothesis that hindered vibrational energy flow can lead to energy localization that enhances chemical reactivity leading to detonation.

Acknowledgment. The authors gratefully acknowledge Dr. Shreve for use of the Raman apparatus, Dr. Hiskey for providing the energetic materials, and Los Alamos National Laboratory Laboratory Directed Research and Development Exploratory Research program for providing funding. This work was performed at Los Alamos National Laboratory under Department of Energy contract W-7405-ENG.

References and Notes

(1) Coffey, C. S.; Toton, E. T. *J. Chem. Phys.* **1982**, *76*, 949.
(2) Walker, F. E. *J. Appl. Phys.* **1988**, *63*, 5548.
(3) Dlott, D. D.; Fayer, M. D. *J. Chem. Phys.* **1990**, *92*, 3798.
(4) Tokmakoff, A.; Fayer, M. D.; Dlott, D. D. *J. Phys. Chem.* **1993**, *97*, 1901.
(5) Fried, L. E.; Ruggiero, A. J. *J. Phys. Chem.* **1994**, *98*, 9786.
(6) Tarver, C. M. *J. Phys. Chem. A* **1997**, *101*, 4845.
(7) Hong, X. Y.; Chen, S.; Dlott, D. D. *J. Phys. Chem.* **1995**, *99*, 9102.
(8) Kim, H.; Dlott, D. D. *J. Chem. Phys.* **1990**, *93*, 1695.
(9) McNesby, K. L.; Coffey, C. S. *J. Phys. Chem. B* **1997**, *101*, 3097.
(10) Ye, S.; Tonokura, K.; Koshi, M. *Kayaku Gakkaishi* **2002**, *63*, 49.
(11) Ye, S.; Tonokura, K.; Koshi, M. *Chem. Phys.* **2003**, *293*, 1.
(12) Ye, S. J.; Tonokura, K.; Koshi, M. *Combust. Flame* **2003**, *132*, 240.
(13) McGrane, S. D.; Shreve, A. P. *J. Chem. Phys.* **2003**, *119*, 5834.
(14) Koshi, M.; Ye, S.; Widijaja, J.; Tonokura, K. *Estimation of shock sensitivity based on molecular properties*; 4th International Symposium on Impact Engineering; July 16−18, 2001; KUMAMOTO, Japan, 2001, KUMAMOTO, Japan.
(15) Califano, S.; Schettino, V.; Neto, N. *Lattice Dynamics of Molecular Crystals*; Springer: New York, 1981.
(16) Bottger, H. *Principles of the Theory of Lattice Dynamics*; Akademie: Berlin, Germany, 1983.
(17) Califano, S.; Schettino, V. *Int. Rev. Phys. Chem.* **1988**, *7*, 19.
(18) Hill, J. R.; Dlott, D. D. *J. Chem. Phys.* **1988**, *89*, 842.
(19) Deopura, B. L.; Gupta, V. D. *J. Chem. Phys.* **1971**, *54*, 4013.
(20) Satija, S. K.; Swanson, B.; Eckert, J.; Goldstone, J. A. *J. Phys. Chem.* **1991**, *95*, 10103.
(21) Towns, T. G. *Spectrochim. Acta, Part A* **1983**, *39*, 801.

(22) Vergoten, G.; Fleury, G.; Blain, M.; Odiot, S. *J. Raman Spectrosc.* **1985**, *16*, 143.
(23) Baharie, E.; Pawley, G. S. *Acta Crystallogr. Sect. A* **1982**, *38*, 803.
(24) Bellows, J. C.; Prasad, P. N. *J. Chem. Phys.* **1979**, *70*, 1864.
(25) Chang, T. C.; Jou, B. H.; Ou, R. S.; Chiang, C. C.; Li, H. W. *Chem. Phys. Lett.* **1991**, *187*, 208.
(26) Crowell, R. A.; Chronister, E. L. *J. Phys. Chem.* **1992**, *96*, 9660.
(27) Dellavalle, R. G.; Fracassi, P. F.; Righini, R.; Califano, S. *Chem. Phys.* **1983**, *74*, 179.
(28) Dlott, D. D.; Schosser, C. L.; Chronister, E. L. *Chem. Phys. Lett.* **1982**, *90*, 386.
(29) Duppen, K.; Hesp, B. M. M.; Wiersma, D. A. *Chem. Phys. Lett.* **1981**, *79*, 399.
(30) Hesp, B. H.; Wiersma, D. A. *Chem. Phys. Lett.* **1980**, *75*, 423.
(31) Hess, L. A.; Prasad, P. N. *J. Chem. Phys.* **1980**, *72*, 573.
(32) Panero, C.; Bini, R.; Schettino, V. *J. Chem. Phys.* **1994**, *100*, 7938.
(33) Ranson, P.; Ouillon, R.; Califano, S. *Chem. Phys.* **1984**, *86*, 115.
(34) Sheka, E. F.; Bokhenkov, E. L.; Dorner, B.; Kalus, J.; Mackenzie, G. A.; Natkaniec, I.; Pawley, G. S.; Schmelzer, U. *J. Phys. C*: *Solid State Phys.* **1984**, *17*, 5893.
(35) Chronister, E. L.; Crowell, R. A. *J. Phys. Chem.* **1991**, *95*, 2420.
(36) Dlott, D. D. *Annu. Rev. Phys. Chem.* **1986**, *37*, 157.
(37) Harris, C. B.; Shelby, R. M.; Cornelius, P. A. *Chem. Phys. Lett.* **1978**, *57*, 8.
(38) Hill, J. R.; Chronister, E. L.; Chang, T. C.; Kim, H.; Postlewaite, J. C.; Dlott, D. D. *J. Chem. Phys.* **1988**, *88*, 949.
(39) Hill, J. R.; Chronister, E. L.; Chang, T. C.; Kim, H.; Postlewaite, J. C.; Dlott, D. D. *J. Chem. Phys.* **1988**, *88*, 2361.
(40) Kosic, T. J.; Cline, R. E.; Dlott, D. D. *J. Chem. Phys.* **1984**, *81*, 4932.
(41) Ouillon, R.; Pinan-Lucarre, J. P.; Ranson, P. *J. Raman Spectrosc.* **2000**, *31*, 605.
(42) Ouillon, R.; Ranson, P.; Califano, S. *Chem. Phys.* **1984**, *91*, 119.
(43) Velsko, S.; Hochstrasser, R. M. *J. Phys. Chem.* **1985**, *89*, 2240.
(44) Maradudin, A. A.; Fein, A. E. *Phys. Rev.* **1962**, *128*, 2589.
(45) Maradudin, A. A.; Fein, A. E.; Vineyard, G. H. *Phys. Status Solidi* **1962**, *2*, 1479.
(46) Dellavalle, R. G.; Venuti, E.; Brillante, A. *Chem. Phys.* **1995**, *198*, 79.
(47) Perrin, B. *Phys. Rev. B*: *Condens. Matter Mater. Phys.* **1987**, *36*, 4706.
(48) DellaValle, R. G.; Signorini, G. F.; Procacci, P. *Phys. Rev. B*: *Condens. Matter Mater. Phys.* **1997**, *55*, 14855.
(49) Becke, A. D. *J. Chem. Phys.* **1993**, *98*, 5648.
(50) Lee, C. T.; Yang, W. T.; Parr, R. G. *Phys. Rev. B* **1988**, *37*, 785.
(51) Ditchfield, R.; Hehre, W. J.; Pople, J. A. *J. Chem. Phys.* **1971**, *54*, 724.
(52) Hehre, W. J.; Ditchfie, R.; Pople, J. A. *J. Chem. Phys.* **1972**, *56*, 2257.
(53) Hehre, W. J.; Pople, J. A. *J. Chem. Phys.* **1972**, *56*, 4233.
(54) Binkley, J. S.; Pople, J. A. *J. Chem. Phys.* **1977**, *66*, 879.
(55) Hariharan, P. C.; Pople, J. A. *Theor. Chim. Acta* **1973**, *28*, 213.
(56) Brand, H. V.; Rabie, R. L.; Funk, D. J.; Diaz-Acosta, I.; Pulay, P. *J. Phys. Chem. B* **2002**, *106*, 10594.
(57) Gruzdkov, Y. A.; Gupta, Y. M. *J. Phys. Chem. A* **2001**, *105*, 6197.
(58) Frisch, M. J.; Trucks, G. W.; Schlegel, H. B.; Scuseria, G. E.; Robb, M. A.; Cheeseman, J. R.; Montgomery, J. A., Jr.; Vreven, T.; Kudin, K. N.; Burant, J. C.; Millam, J. M.; Iyengar, S. S.; Tomasi, J.; Barone, V.; Mennucci, B.; Cossi, M.; Scalmani, G.; Rega, N.; Petersson, G. A.; Nakatsuji, H.; Hada, M.; Ehara, M.; Toyota, K.; Fukuda, R.; Hasegawa, J.; Ishida, M.; Nakajima, T.; Honda, Y.; Kitao, O.; Nakai, H.; Klene, M.; Li, X.; Knox, J. E.; Hratchian, H. P.; Cross, J. B.; Bakken, V.; Adamo, C.; Jaramillo, J.; Gomperts, R.; Stratmann, R. E.; Yazyev, O.; Austin, A. J.; Cammi, R.; Pomelli, C.; Ochterski, J. W.; Ayala, P. Y.; Morokuma, K.; Voth, G. A.; Salvador, P.; Dannenberg, J. J.; Zakrzewski, V. G.; Dapprich, S.; Daniels, A. D.; Strain, M. C.; Farkas, O.; Malick, D. K.; Rabuck, A. D.; Raghavachari, K.; Foresman, J. B.; Ortiz, J. V.; Cui, Q.; Baboul, A. G.; Clifford, S.; Cioslowski, J.; Stefanov, B. B.; Liu, G.; Liashenko, A.; Piskorz, P.; Komaromi, I.; Martin, R. L.; Fox, D. J.; Keith, T.; Al-Laham, M. A.; Peng, C. Y.; Nanayakkara, A.; Challacombe, M.; Gill, P. M. W.; Johnson, B.; Chen, W.; Wong, M. W.; Gonzalez, C.; Pople, J. A. *Gaussian 03*, Revision B.04; Gaussian, Inc: Wallingford, CT, 2004.
(59) Manaa, M. R.; Fried, L. E. *J. Phys. Chem. A* **2001**, *105*, 6765.
(60) Cady, H. H.; Larson, A. C. *Acta Crystallogr. Sect. B*: *Struct. Sci.* **1975**, *31*, 1864.
(61) Cady, H. W.; Larson, A. C. *Acta Crystallogr. Sect. A* **1965**, *18*, 485.
(62) Choi, C. S.; Boutin, H. P. *Acta Crystallogr. Sect. B*: *Struct. Crystallogr. Cryst. Chem.* **1970**, *B26*, 1235.
(63) Booth, A. D.; Llewellyn, F. J. *J. Chem. Soc.* **1947**, 837.
(64) Abrahams, S. C.; Robertson, J. M.; White, J. G. *Acta Crystallogr.* **1949**, *2*, 233.
(65) Martin, W. C.; Fuhr, J. R.; Kelleher, D. E.; Musgrove, A.; Sugar, J.; Wiese, W. L.; Mohr, P. J.; Olsen, K. NIST Atomic Spectra Database (version 2.0), available online http://physics.nist.gov/asd2; National Institute of Standards and Technology, Gaithersburg, MD, 1999.
(66) Gibbs, T. R.; Popolato, A. *LASL Explosive Property Data*; University of California Press: Berkeley, CA, 1980.